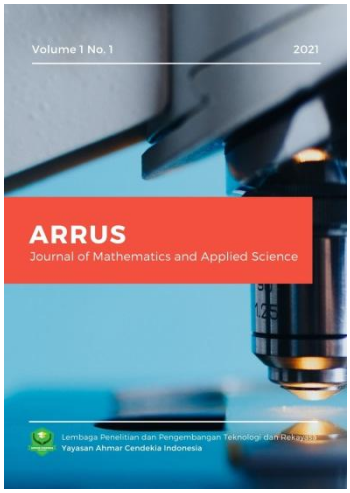
https://doi.org/10.35877/mathscience5506

OPEN ACCESS

ISSN : 2776-7922 (Print) / 2807-3037 (Online)



*Corresponding author: Sitti Masyitah Meliyana, Universitas Negeri Makassar, Makassar, Indonesia

E-mail: sittimasyitahmr@unm.ac.id

RESEARCH ARTICLE

Land Cover Change in the Mamminasata Metropolitan Area, Indonesia, 2005–2025 and CA-Markov Prediction for 2035

Sitti Masyitah Meliyana*, Agung Tri Utomo,& Muh. Qodri Alfairus

Universitas Negeri Makassar, Makassar, South Sulawesi, Indonesia.

Abstract: This study examines land cover change in the Mamminasata Metropolitan Area (Makassar, Maros, Gowa, and Takalar), South Sulawesi, Indonesia, between 2005 and 2025 and projects its land cover to 2035. Landsat 5 TM and Landsat 8/9 OLI surface reflectance composites were classified into seven classes on Google Earth Engine using a Random Forest classifier trained with samples derived automatically from Dynamic World labels, followed by rule-based post-classification and temporal consistency corrections. Future land cover was simulated with a CA-Markov model that combines Markov transition quantities, a gradient boosting suitability model, and cellular automata allocation. The classified maps reached overall accuracies of 77.9% (2005), 81.6% (2015), and 84.9% (2025), and the 2025 hindcast agreed with the observed map at 87.3% (Kappa 0.82; Figure of Merit 0.13). Built-up land expanded from 38,036 ha to 60,661 ha (+59.5%), while paddy fields declined by 9,457 ha (−15.1%). Dryland farms and shrubland supplied 55.3% and paddy fields 29.0% of the new built-up land in 2015–2025, and 61% of the 2005–2025 growth occurred more than 20 km from the city centre. Under a business-as-usual trend, built-up land will reach 71,293 ha in 2035, mainly within 5–15 km of the city centre, and paddy fields will fall to 48,924 ha. The findings indicate that urban growth in Mamminasata has shifted from the core city to its agricultural periphery.

Keywords: Land Cover Change, Random Forest, CA-Markov, Google Earth Engine, Mamminasata

1. Introduction

Rapid urbanization in developing countries converts large areas of agricultural and natural land into built-up land, often faster than spatial planning can respond. In East and Southeast Asia, urban land expanded markedly during 2000–2010, mostly at the expense of cropland surrounding existing cities (Schneider et al., 2015). In Indonesia, this process is most visible in metropolitan regions where the core city has limited land and new housing, industry, and infrastructure spill over into neighbouring regencies. Studies of Jabodetabek show that peri-urban agriculture shrinks and changes form under such pressure (Pribadi & Pauleit, 2015), while evidence from East Java shows that housing on converted farmland can be worth about seven times more than the farmland itself, which explains why conversion is hard to stop (Rondhi et al., 2018).

The Mamminasata Metropolitan Area, formed by Makassar City and the regencies of Maros, Gowa, and Takalar, is one of the largest urban agglomerations in eastern Indonesia and a national strategic area for development. Previous studies have documented rapid land use

This open access article is distributed under a Creative Commons Attribution (CC-BY-NC) 4.0 license.

https://doi.org/10.35877/mathscience5506

ISSN : 2776-7922 (Print) / 2807-3037 (Online)

change in parts of this region. Surya et al. (2020) reported that paddy fields in the Hertasning–Samata corridor fell from 397 ha in 2001 to 46 ha in 2019 as settlements expanded, and Surya et al. (2021) estimated that about 5,881 ha of productive farmland in northern Makassar was converted between 2006 and 2020. Arifin et al. (2023) projected that built-up land in the peri-urban north of Makassar would cover 67% of that area by 2031. In Maros, 1,946 ha of paddy fields were lost between 2013 and 2023 (Munawir et al., 2023), and in Gowa, Random Forest classification on Google Earth Engine showed that vegetation has been largely replaced by built-up land (Jannah & Arif, 2025).

These studies, however, focus on individual districts, corridors, or a single regency, and most compare only two dates. A consistent, metropolitan-wide picture of land cover change over two decades, together with a validated projection of future change, is still missing. Such a picture matters because the conversion of paddy fields and aquaculture ponds in Maros and Takalar affects regional food production, while the loss of forest in upland Gowa affects the water supply of the whole metropolitan area.

Cloud-based platforms now make such analysis feasible. Google Earth Engine (GEE) provides the full Landsat archive and parallel processing (Gorelick et al., 2017), and the Dynamic World product supplies near real-time global land cover labels that can support the collection of training data (Brown et al., 2022). Combined with Random Forest classification (Breiman, 2001) and CA-Markov modelling, these resources allow consistent long-term mapping and projection over large areas without extensive field campaigns.

This study therefore aims to (1) map land cover in the Mamminasata Metropolitan Area in 2005, 2015, and 2025 using a consistent GEE workflow, (2) quantify the magnitude, sources, and spatial pattern of land cover change, particularly the growth of built-up land and the loss of paddy fields, and (3) project land cover in 2035 with a validated CA-Markov model. The study contributes a reproducible, metropolitan-scale analysis that can inform the protection of agricultural land and the direction of urban growth in the region.

2. Literature Review

2.1. *Urban expansion and agricultural land conversion*

Urban expansion in Indonesian metropolitan regions typically proceeds from the core city towards its fringe, where land is cheaper and still largely agricultural. In the Makassar–Gowa fringe, commercial functions and capital-driven housing development reshape the spatial structure and accelerate the conversion of paddy fields (Surya, 2016). Gated communities have spread across Mamminasata in an irregular pattern, with 392 such developments identified, and they fragment the surrounding agricultural landscape (Indradjati & Ramli, 2021). Along the coast of Makassar, population growth has reduced open areas while built-up land increased (Nganro et al., 2024). Similar dynamics have been described for other Indonesian metropolitan areas, where peri-urban farmland persists only in fragmented and transformed forms (Pribadi & Pauleit, 2015). The economic advantage of residential use over farming in peri-urban locations is a key driver of this conversion (Rondhi et al., 2018).

2.2. *Land cover classification with Random Forest and Google Earth Engine*

Random Forest is an ensemble of decision trees grown on bootstrap samples with random subsets of predictors (Breiman, 2001). In remote sensing, it produces high classification accuracy, handles many correlated predictors, and is relatively insensitive to its parameters, although it is sensitive to imbalanced training samples (Belgiu & Drăguţ, 2016). Landsat Collection 2 provides geometrically and radiometrically consistent surface reflectance from Landsat 5 TM to Landsat 9 OLI-2, which makes multi-decadal comparisons more reliable (Crawford et al., 2023). Spectral indices such as the Normalized Difference Built-up Index (NDBI) and the Modified Normalized Difference Water Index (MNDWI) improve the separation of built-up and water surfaces (Xu, 2006; Zha et al., 2003). On GEE, these data

This open access article is distributed under a Creative Commons Attribution (CC-BY-NC) 4.0 license.

https://doi.org/10.35877/mathscience5506

ISSN : 2776-7922 (Print) / 2807-3037 (Online)

and algorithms can be applied over an entire metropolitan region in a single workflow (Gorelick et al., 2017).

Collecting training data is often the most costly step of classification. The Dynamic World product provides 10 m land cover labels with per-pixel class probabilities derived from Sentinel-2 imagery (Brown et al., 2022). Its labels can be used as a source of training samples when they are filtered for temporal consistency and spatial homogeneity, but accuracy measured against such labels is not equivalent to accuracy measured against field data. Good practice therefore requires transparent reporting of the sampling design and error matrix (Congalton & Green, 2019; Olofsson et al., 2014).

2.3. CA-Markov modelling of land cover change

The CA-Markov approach combines a Markov chain, which estimates how much land moves between classes over a period, with cellular automata, which decide where those changes occur based on transition suitability and neighbourhood effects. It has been widely applied to project urban growth, for example in Iraq (Hamad et al., 2018), Oman (Mansour et al., 2020), and the Indonesian city of Banjarmasin (Supriatna et al., 2022). Recent studies replace the classical multi-criteria suitability maps with machine-learning models such as artificial neural networks in the MOLUSCE plugin (Muhammad et al., 2022). Gradient boosting (Friedman, 2001), particularly its fast histogram-based implementations (Ke et al., 2017; Pedregosa et al., 2011), offers another option that handles non-linear effects of distance and terrain variables.

Model validation is essential before a projection is interpreted. Kappa and overall agreement are dominated by unchanged land and can therefore look high even for poor change predictions (Pontius & Millones, 2011). The Figure of Merit (FoM), which measures the overlap between observed and simulated change, provides a stricter test; a comparison of 13 land change models found that most had an FoM below 50% (Pontius et al., 2008).

3. Research Method and Materials

3.1. Study area

The study area is the Mamminasata Metropolitan Area in South Sulawesi Province, Indonesia, which comprises Makassar City and the regencies of Maros, Gowa, and Takalar (approximately 4°42'–5°38' S and 119°20'–120°03' E). The region stretches from the coastal lowlands along the Makassar Strait, dominated by settlements, paddy fields, and aquaculture ponds, to the volcanic highlands of Gowa, which rise to about 2,880 m. Administrative boundaries were taken from the FAO Global Administrative Unit Layers (level 2) and extended by a 2 km buffer seaward to include the coastline and coastal ponds. The analysis domain covers 471,341 ha. All data were projected to WGS 84 / UTM zone 50S at 30 m resolution.

3.2. Data and image preprocessing

Landsat Collection 2 Level-2 surface reflectance images were processed on GEE: Landsat 5 TM for 2005 and Landsat 8 and 9 OLI for 2015 and 2025 (Crawford et al., 2023). Clouds, cloud shadows, and saturated pixels were removed using the QA_PIXEL band. For each target year, a median composite of dry-season images (June–October) was built from a window of ±1 year. Because cloud-free Landsat 5 coverage was limited, the window for 2005 was widened to 2003–2007. Pixels that remained empty were filled with a composite of all months within ±4 years. Elevation and slope were derived from the 30 m Shuttle Radar Topography Mission (SRTM) digital elevation model.

Each composite was stacked with six reflectance bands (blue, green, red, near-infrared, and two shortwave infrared bands), three spectral indices, the 10th and 90th percentiles of annual NDVI and MNDWI to capture the phenology of paddy fields and the inundation of ponds,

This open access article is distributed under a Creative Commons Attribution (CC-BY-NC) 4.0 license.

https://doi.org/10.35877/mathscience5506

ISSN : 2776-7922 (Print) / 2807-3037 (Online)

NDVI and MNDWI of a wet-season (January–April) composite, and the two terrain variables. The indices were computed as follows:

$$NDVI = (NIR - Red) / (NIR + Red) \quad (1)$$

$$NDBI = (SWIR1 - NIR) / (SWIR1 + NIR) \quad (2)$$

$$MNDWI = (Green - SWIR1) / (Green + SWIR1) \quad (3)$$

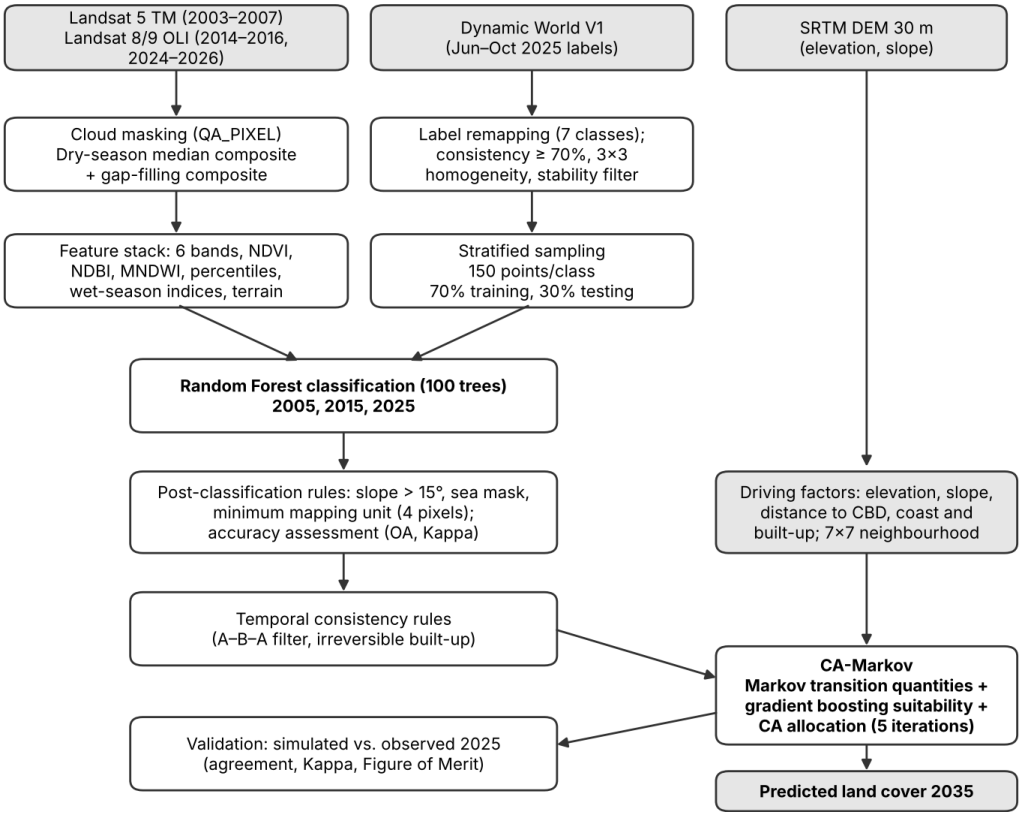


Figure 1. Research workflow

3.3. *Classification scheme and training data*

Land cover was mapped into seven classes: built-up land, paddy fields, aquaculture ponds, water bodies, forest, dryland farms and shrubland, and bare land. Training and testing samples were generated automatically from the Dynamic World V1 product (Brown et al., 2022) for June–October 2025. The modal Dynamic World label was remapped to the seven classes: built area to built-up land; crops and flooded vegetation to paddy fields; water on land below 5 m elevation to aquaculture ponds and other water to water bodies; trees below 100 m elevation to dryland farms and shrubland (mixed tree gardens) and other trees to forest; grass and shrub to dryland farms and shrubland; and bare ground to bare land. Unlabelled sea pixels in the coastal buffer were added to water bodies where MNDWI exceeded 0.2.

Three filters were applied to obtain reliable samples. First, the modal label had to occur in at least 70% of the Dynamic World observations of the period. Second, the pixel had to be homogeneous within a 3 × 3 window. Third, because Dynamic World is only available from 2015 onwards, samples for 2005 and 2015 were restricted to pixels whose spectral indices differed by less than 0.15 from the 2025 composite, so that the 2025 labels could be transferred to stable pixels. From the eligible pixels, 150 points per class were drawn by stratified random sampling and split randomly into 70% for training and 30% for testing.

This open access article is distributed under a Creative Commons Attribution (CC-BY-NC) 4.0 license.

https://doi.org/10.35877/mathscience5506

ISSN : 2776-7922 (Print) / 2807-3037 (Online)

3.4. *Classification and post-classification correction*

Each year was classified with a Random Forest of 100 trees and a minimum leaf population of two (Belgiu & Drăguţ, 2016; Breiman, 2001). Three rules were then applied to correct systematic errors. Built-up pixels on slopes steeper than 15° were reassigned to bare land if NDVI was below 0.3 and to dryland farms and shrubland otherwise, because dense settlement is rare on steep volcanic slopes in the study area. Pixels at or below 0 m elevation classified as paddy fields, ponds, or dryland farms were reassigned to water bodies (sea). Finally, patches smaller than four pixels (0.36 ha) were replaced by the majority class of their neighbourhood.

3.5. *Accuracy assessment*

Accuracy was assessed on the final, corrected maps using the 30% testing samples. Overall accuracy (OA) and the Kappa coefficient were derived from the error matrix (Congalton & Green, 2019). Because the reference labels come from Dynamic World rather than field observations, the reported accuracy measures agreement with an independent global product and should be interpreted accordingly (Olofsson et al., 2014).

3.6. *Temporal consistency*

Because each year was classified independently, part of the apparent change between maps is caused by classification error. Two rules were applied to reduce this pseudo-change. First, an A–B–A sequence (the same class in 2005 and 2025 but a different class in 2015) was treated as an error in 2015, and the 2015 class was set to that of 2005 and 2025. Second, built-up land was considered irreversible. Using the 2025 map, which has the highest accuracy, as the reference, built-up pixels in an earlier year that were not built-up in the following year were treated as errors and replaced with the class of the following year.

3.7. *CA-Markov modelling and validation*

The CA-Markov model consisted of three components. A Markov chain determined the quantity of change: the transition probability matrix was obtained by cross-tabulating two maps ten years apart and multiplied by the area of each class at the start of the period to obtain the number of pixels moving from class i to class j. A transition suitability model determined where change was likely: a histogram-based gradient boosting classifier (200 iterations, learning rate 0.1) was trained on 300,000 random pixels to predict the class at the end of the period (Friedman, 2001; Ke et al., 2017; Pedregosa et al., 2011). Its predictors were elevation, slope, distance to the city centre (Karebosi Square, Makassar), distance to the coastline, distance to the nearest built-up pixel, the proportion of each class within a 7 × 7 pixel neighbourhood, and the class at the start of the period. Cellular automata then allocated the Markov quantities in five iterations, each representing two years; in each iteration, the quota of each class pair was assigned to the candidate pixels with the highest suitability, and the neighbourhood and distance variables were recalculated.

The model was calibrated with the 2005 and 2015 maps to simulate 2025, and the simulation was compared with the classified 2025 map. Overall agreement, Kappa, and the Figure of Merit were calculated (Pontius et al., 2008; Pontius & Millones, 2011):

$$\mathrm{FoM} = H / (M + H + W + F) \tag{4}$$

where H (hits) is observed change simulated correctly, M (misses) is observed change simulated as persistence, W (wrong hits) is observed change simulated to the wrong class, and F (false alarms) is observed persistence simulated as change. After validation, the model was recalibrated with the 2015 and 2025 maps and used to project land cover in 2035 under a business-as-usual scenario. The modelling was implemented in Python with NumPy, SciPy, rasterio, and scikit-learn. The full workflow is summarized in Figure 1.

4. Results and Discussion

This open access article is distributed under a Creative Commons Attribution (CC-BY-NC) 4.0 license.

https://doi.org/10.35877/mathscience5506

ISSN : 2776-7922 (Print) / 2807-3037 (Online)

4.1. Results

4.1.1. Classification accuracy

All three maps reached overall accuracies between 77.9% and 84.9% and Kappa coefficients between 0.75 and 0.82 (Table 1). Accuracy increased from 2005 to 2025, which reflects both the better radiometric quality of Landsat OLI compared with TM and the shorter time gap between the image date and the Dynamic World reference. The most frequent confusions occurred between spectrally similar classes. In 2015, paddy fields and water bodies had the lowest class-level accuracies (66% and 68%), mainly because flooded paddy fields resemble ponds and shallow water; in 2005, water bodies were frequently confused with bare land. These accuracies are lower than the Kappa of 0.90 reported for a two-date classification of Gowa (Jannah & Arif, 2025), which used fewer classes, but they are adequate for analysing class-level change at the metropolitan scale.

Table 1. Classification accuracy and CA-Markov validation

Map	Sensor	Image window	Overall accuracy / agreement (%)	Kappa
Classified 2005	Landsat 5 TM	2003–2007	77.9	0.75
Classified 2015	Landsat 8 OLI	2014–2016	81.6	0.76
Classified 2025	Landsat 8/9 OLI	2024–2026	84.9	0.82
Simulated 2025 (CA-Markov)	–	Calibrated 2005–2015	87.3	0.82

Note: Classification accuracy was assessed against Dynamic World-derived test samples; the simulated 2025 map was compared with the classified 2025 map (Figure of Merit = 0.128).

4.1.2. Land cover dynamics, 2005–2025

Built-up land was the fastest-growing class. It increased by 22,625 ha (59.5%), from 38,036 ha in 2005 to 60,661 ha in 2025, an average of about 1,131 ha per year (Table 2). The increase was similar in both decades, 11,623 ha in 2005–2015 and 11,002 ha in 2015–2025, but because the base was larger the annual growth rate fell from 2.70% to 2.02%. Paddy fields declined steadily by 4,895 ha and 4,562 ha in the two decades, a loss of 9,457 ha (15.1%) over twenty years or about 0.8% per year. Aquaculture ponds decreased by 10.5%, mostly in the second decade.

Forest remained the largest class, covering about 45% of the area, and changed little in net terms (−1.0%). This stability hides substantial two-way exchange: about 7,400–8,600 ha of forest became dryland farms and shrubland in each decade, while 5,900–6,400 ha moved in the opposite direction, which is consistent with rotational cultivation and tree gardens in the uplands of Gowa and Maros. The decline of water bodies between 2005 and 2015 (−9,383 ha) came mostly from pixels classified as water in 2005 that became dryland farms, paddy fields, and forest in 2015. Given the low accuracy of the water class in 2005 and the strong seasonal inundation of the lowlands, this change is interpreted mainly as a classification artefact rather than a real loss of water.

Table 2. Land cover area in 2005, 2015, 2025, and predicted 2035 (ha)

Land cover class	2005	2015	2025	2035 (predicted)	Change 2005–2025 (%)	Change 2025–2035 (%)
Built-up land	38,036	49,659	60,661	71,293	+59.5	+17.5
Paddy fields	62,451	57,556	52,994	48,924	−15.1	−7.7
Aquaculture ponds	3,717	3,940	3,327	2,841	−10.5	−14.6
Water bodies	36,945	27,562	26,735	25,938	−27.6	−3.0
Forest	213,178	213,659	211,074	208,369	−1.0	−1.3
Dryland farms/shrubland	110,068	114,667	111,500	108,473	+1.3	−2.7
Bare land	6,947	4,297	5,049	5,504	−27.3	+9.0
Total	471,341	471,341	471,341	471,341		

Note: Areas are computed over the full analysis domain, including a 2 km coastal buffer.

4.1.3. Sources of new built-up land

This open access article is distributed under a Creative Commons Attribution (CC-BY-NC) 4.0 license.

https://doi.org/10.35877/mathscience5506

ISSN : 2776-7922 (Print) / 2807-3037 (Online)

The transition matrix for 2015–2025 (Table 3) shows where the new built-up land came from. Of the 11,002 ha of new built-up land, 6,079 ha (55.3%) came from dryland farms and shrubland, 3,190 ha (29.0%) from paddy fields, and 887 ha (8.1%) from forest. In 2005–2015, paddy fields supplied a larger share, 4,138 ha of the 11,623 ha of new built-up land (35.6%). In terms of Markov probabilities, 5.5% of paddy fields and 5.3% of dryland farms became built-up within one decade, while bare land had the highest probability (10.2%), because cleared land in the fringe is usually the first stage of construction. About 21.8% of aquaculture ponds turned into paddy fields, reflecting the rotation between ponds and paddy cultivation on the coastal plains of Maros and Takalar.

Table 3. Land cover transition matrix, 2015–2025 (ha)

2015 \ 2025	Built-up	Paddy	Ponds	Water	Forest	Dryland/ shrub	Bare	Total 2015
Built-up land	49,659	0	0	0	0	0	0	49,659
Paddy fields	3,190	49,122	180	99	910	2,986	1,070	57,556
Aquaculture ponds	26	859	3,006	7	0	11	32	3,940
Water bodies	381	442	124	26,322	28	22	243	27,562
Forest	887	382	0	57	203,700	8,610	23	213,659
Dryland farms/shrubland	6,079	2,008	14	209	6,392	99,508	457	114,667
Bare land	439	180	3	43	44	363	3,224	4,297
Total 2025	60,661	52,994	3,327	26,735	211,074	111,500	5,049	471,341

Note: Rows are classes in 2015 and columns are classes in 2025; diagonal values are persistence.

4.1.4. Spatial pattern of urban expansion

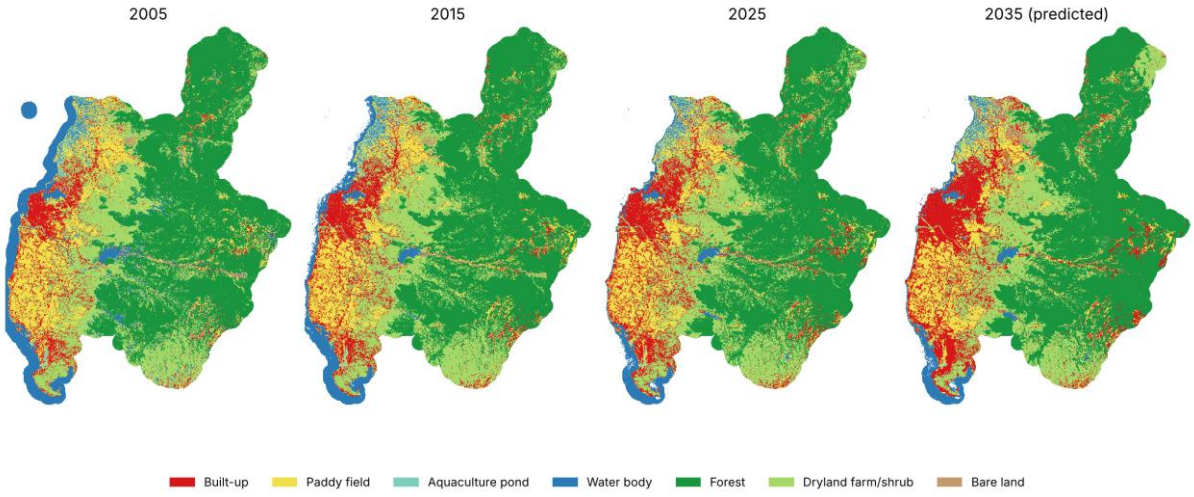


Figure 2. Land cover of the Mamminasata Metropolitan Area in 2005, 2015, 2025, and predicted 2035

Figure 2 shows that built-up land in 2005 was concentrated in Makassar and along the main roads to Maros in the north and Sungguminasa (Gowa) in the south-east. By 2025, settlements had merged into a continuous urban belt along these corridors and had expanded across the coastal plain of Takalar. Table 4 summarizes this pattern by distance from the city centre. Within 5 km, built-up land already covered 66.7% of the land in 2005 and 76.2% in 2025, leaving little room for further growth. The largest relative gains occurred in the 5–15 km zones, where the built-up share rose from 40.0% to 58.4% (5–10 km) and from 22.2% to 35.2% (10–15 km).

Most of the new built-up land, however, appeared far from the centre. Areas more than 20 km from Karebosi received 61.0% of the built-up growth in 2005–2025, even though their built-up share remained low (6.6–14.3% in 2025). This reflects a dispersed growth pattern

This open access article is distributed under a Creative Commons Attribution (CC-BY-NC) 4.0 license.

https://doi.org/10.35877/mathscience5506

ISSN : 2776-7922 (Print) / 2807-3037 (Online)

along regional roads, around the district towns of Maros, Sungguminasa, and Takalar, and in scattered villages, rather than a compact expansion of the core city. Such leapfrog development is consistent with the irregular spread of gated communities reported for Mamminasata (Indradjati & Ramli, 2021) and with the fringe-driven growth described for the Makassar–Gowa border (Surya, 2016; Surya et al., 2020).

Table 4. Built-up land by distance from the city centre (Karebosi Square, Makassar)

Distance zone (km)	Land area (ha)	Built-up 2005 (%)	Built-up 2025 (%)	Built-up 2035 (%)	Share of new built-up 2005–2025 (%)	Share of new built-up 2025–2035 (%)
0–5	7,385	66.7	76.2	83.2	3.1	4.8
5–10	14,082	40.0	58.4	72.9	11.5	19.6
10–15	20,752	22.2	35.2	45.6	11.9	20.2
15–20	28,705	14.2	24.1	26.9	12.6	7.4
20–30	78,436	7.9	14.3	15.7	22.0	10.2
> 30	322,380	3.9	6.6	7.9	39.0	37.8

Note: Built-up percentages are relative to the land area of each zone; shares of new built-up land sum to 100% for each period.

4.1.5. Model validation and land cover prediction for 2035

The CA-Markov model calibrated on 2005–2015 reproduced the 2025 map with an overall agreement of 87.3% and a Kappa of 0.82 (Table 1). The Figure of Merit was 0.128. Of the 36,800 ha that actually changed between 2015 and 2025, 8,765 ha were simulated correctly, 2,860 ha were simulated to the wrong class, and 25,175 ha were missed, while 31,624 ha were false alarms. The model was much better at predicting how much change would occur than where: it simulated 10,832 ha of new built-up land against 11,002 ha observed, a difference of only 1.6%, but only 2,338 ha of it fell on the correct pixels. An FoM of this level is common for land change models, most of which score below 0.5, and low values are expected when the observed change is a small fraction of the landscape, here 7.8% in ten years (Pontius et al., 2008). The projection should therefore be read as a reliable estimate of the quantity of change and of its general spatial tendency, not as a pixel-level forecast.

If the 2015–2025 trend continues, built-up land will reach 71,293 ha in 2035, an increase of 10,632 ha (17.5%) and 15.1% of the study area (Table 2). Paddy fields will shrink by a further 4,070 ha (7.7%) to 48,924 ha, of which 2,937 ha will be converted directly to built-up land, and aquaculture ponds will lose 14.6% of their area. In contrast to the dispersed growth of the past two decades, the model allocates 39.8% of new built-up land to the 5–15 km zones (Table 4), where the built-up share will reach 72.9% (5–10 km) and 45.6% (10–15 km). This concentration results from the neighbourhood and distance-to-built-up variables, which favour growth adjacent to existing settlements, and indicates that the remaining paddy fields of the inner fringe are the most exposed to conversion.

4.2. Discussion

The results confirm, at the metropolitan scale, the conversion trends reported in local studies. The steady loss of roughly 450 ha of paddy fields per year agrees with the 1,946 ha lost in Maros alone during 2013–2023 (Munawir et al., 2023), and the strong increase of built-up land in the 5–15 km zones matches the farmland conversion documented in northern Makassar and the Hertasning–Samata corridor (Surya et al., 2020, 2021). The projected built-up share in the inner fringe is lower than the 67% projected by Arifin et al. (2023) for 2031, but their study covered only the peri-urban districts of northern Makassar, where urbanization is most advanced; our 5–10 km zone, which includes these districts, reaches a comparable 72.9% in 2035.

Two features of the change deserve attention from planners. First, dryland farms and shrubland, rather than paddy fields, supplied the majority of new built-up land after 2015. This suggests that the protection of irrigated paddy fields may have shifted part of the development pressure to rainfed land and mixed gardens, which are less regulated but still

This open access article is distributed under a Creative Commons Attribution (CC-BY-NC) 4.0 license.

ISSN : 2776-7922 (Print) / 2807-3037 (Online)

important for local livelihoods and for water infiltration. Second, the large share of growth more than 20 km from the centre indicates that urbanization is no longer confined to the Makassar fringe but is spreading to district towns and road corridors throughout Maros, Gowa, and Takalar. Dispersed development of this kind raises the cost of infrastructure and fragments agricultural land, as also observed in other Indonesian metropolitan regions (Pribadi & Pauleit, 2015).

Methodologically, the study shows that Dynamic World labels, when filtered for consistency, homogeneity, and spectral stability, can replace manual sample collection and still yield accuracies of about 78–85% for a seven-class scheme. Post-classification rules and temporal consistency checks were essential: without them, built-up land appeared on steep volcanic slopes, coastal sea pixels were labelled as ponds, and built-up land appeared to shrink between years, all of which would have biased the Markov transition matrix.

Several limitations should be noted. Accuracy was measured against Dynamic World labels rather than field data, so the errors of that product are inherited. The 2005 map relies on a wider image window and has the lowest accuracy, particularly for water bodies. Some pseudo-change may remain despite the consistency rules. Finally, the 2035 projection is a business-as-usual scenario that does not include spatial plans, protected areas, or new infrastructure such as toll roads and the Makassar–Parepare railway; scenario-based simulations that incorporate these factors are a natural next step.

5. Conclusion

Between 2005 and 2025, built-up land in the Mamminasata Metropolitan Area increased by 59.5%, from 38,036 ha to 60,661 ha, while paddy fields declined by 15.1% and aquaculture ponds by 10.5%. Growth proceeded at a steady pace of about 11,000 ha per decade and drew increasingly on dryland farms and shrubland, which supplied 55.3% of new built-up land in 2015–2025, while paddy fields supplied 29.0%. Most of the new built-up land appeared more than 20 km from the city centre, which shows that urbanization has spread from Makassar to the surrounding regencies. The validated CA-Markov model, with an overall agreement of 87.3%, projects that built-up land will reach 71,293 ha in 2035 and paddy fields will decline to 48,924 ha, with growth concentrated in the 5–15 km fringe of Makassar. The combination of Google Earth Engine, Random Forest with automatically derived training samples, and a machine-learning CA-Markov model provides a reproducible way to monitor and anticipate land cover change at the metropolitan scale.

References

Arifin, T., Amri, S. N., Rahmania, R., Yulius, Ramdhan, M., Chandra, H., Adrianto, L., Bengen, D. G., Kurniawan, F., & Kurnia, R. (2023). Forecasting land-use changes due to coastal city development on the peri-urban area in Makassar City, Indonesia. The Egyptian Journal of Remote Sensing and Space Science, 26(1), 197–206. https://doi.org/10.1016/j.ejrs.2023.02.002

Belgiu, M., & Drăguţ, L. (2016). Random forest in remote sensing: A review of applications and future directions. ISPRS Journal of Photogrammetry and Remote Sensing, 114, 24–31. https://doi.org/10.1016/j.isprsjprs.2016.01.011

Breiman, L. (2001). Random forests. Machine Learning, 45(1), 5–32. https://doi.org/10.1023/A:1010933404324

Brown, C. F., Brumby, S. P., Guzder-Williams, B., Birch, T., Hyde, S. B., Mazzariello, J., Czerwinski, W., Pasquarella, V. J., Haertel, R., Ilyushchenko, S., Schwehr, K., Weisse, M., Stolle, F., Hanson, C., Guinan, O., Moore, R., & Tait, A. M. (2022). Dynamic World, near real-time global 10 m land use land cover mapping. Scientific Data, 9(1), Article 251. https://doi.org/10.1038/s41597-022-01307-4

Congalton, R. G., & Green, K. (2019). Assessing the accuracy of remotely sensed data: Principles and practices (3rd ed.). CRC Press. https://doi.org/10.1201/9780429052729

This open access article is distributed under a Creative Commons Attribution (CC-BY-NC) 4.0 license.

ISSN : 2776-7922 (Print) / 2807-3037 (Online)

Crawford, C. J., Roy, D. P., Arab, S., Barnes, C., Vermote, E., Hulley, G., Gerace, A., Choate, M., Engebretson, C., Micijevic, E., Schmidt, G., Anderson, C., Anderson, M., Bouchard, M., Cook, B., Dittmeier, R., Howard, D., Jenkerson, C., Kim, M., . . . Zahn, S. (2023). The 50-year Landsat collection 2 archive. Science of Remote Sensing, 8, Article 100103. https://doi.org/10.1016/j.srs.2023.100103

Friedman, J. H. (2001). Greedy function approximation: A gradient boosting machine. The Annals of Statistics, 29(5), 1189–1232. https://doi.org/10.1214/aos/1013203451

Gorelick, N., Hancher, M., Dixon, M., Ilyushchenko, S., Thau, D., & Moore, R. (2017). Google Earth Engine: Planetary-scale geospatial analysis for everyone. Remote Sensing of Environment, 202, 18–27. https://doi.org/10.1016/j.rse.2017.06.031

Hamad, R., Balzter, H., & Kolo, K. (2018). Predicting land use/land cover changes using a CA-Markov model under two different scenarios. Sustainability, 10(10), Article 3421. https://doi.org/10.3390/su10103421

Indradjati, P. N., & Ramli, P. (2021). Dampak spasial komunitas berpagar terhadap kawasan perkotaan Mamminasata [Spatial impacts of gated communities on the Mamminasata urban area]. Tataloka, 23(3), 329–343. https://doi.org/10.14710/tataloka.23.3.329-343

Jannah, M., & Arif, S. (2025). Analysis of land use and land cover change (LULC) in Gowa Regency using multi-temporal satellite imagery. IOP Conference Series: Earth and Environmental Science, 1525(1), Article 012034. https://doi.org/10.1088/1755-1315/1525/1/012034

Ke, G., Meng, Q., Finley, T., Wang, T., Chen, W., Ma, W., Ye, Q., & Liu, T.-Y. (2017). LightGBM: A highly efficient gradient boosting decision tree. In Advances in Neural Information Processing Systems 30 (pp. 3146–3154). Curran Associates. https://proceedings.neurips.cc/paper/2017/hash/6449f44a102fde848669bdd9eb6b76fa-Abstract.html

Mansour, S., Al-Belushi, M., & Al-Awadhi, T. (2020). Monitoring land use and land cover changes in the mountainous cities of Oman using GIS and CA-Markov modelling techniques. Land Use Policy, 91, Article 104414. https://doi.org/10.1016/j.landusepol.2019.104414

Muhammad, R., Zhang, W., Abbas, Z., Guo, F., & Gwiazdzinski, L. (2022). Spatiotemporal change analysis and prediction of future land use and land cover changes using QGIS MOLUSCE plugin and remote sensing big data: A case study of Linyi, China. Land, 11(3), Article 419. https://doi.org/10.3390/land11030419

Munawir, M., Abdullah, N., & Ashari, A. F. (2023). Arahan dan strategi perlindungan lahan sawah untuk mendukung ketahanan pangan di Kabupaten Maros, Sulawesi Selatan [Direction and strategies for protection of rice fields to support food security in Maros Regency, South Sulawesi]. Jurnal Ecosolum, 12(2), 145–162. https://doi.org/10.20956/ecosolum.v12i2.29948

Nganro, S., Nas, W., & Manyila, S. S. (2024). The impact of population growth on open area in the coastal area of Makassar City. Journal of Asian Geography, 3(2), 70–75. https://doi.org/10.36777/jag2024.3.2.7

Olofsson, P., Foody, G. M., Herold, M., Stehman, S. V., Woodcock, C. E., & Wulder, M. A. (2014). Good practices for estimating area and assessing accuracy of land change. Remote Sensing of Environment, 148, 42–57. https://doi.org/10.1016/j.rse.2014.02.015

Pedregosa, F., Varoquaux, G., Gramfort, A., Michel, V., Thirion, B., Grisel, O., Blondel, M., Prettenhofer, P., Weiss, R., Dubourg, V., Vanderplas, J., Passos, A., Cournapeau, D., Brucher, M., Perrot, M., & Duchesnay, É. (2011). Scikit-learn: Machine learning in Python. Journal of Machine Learning Research, 12, 2825–2830. https://jmlr.org/papers/v12/pedregosa11a.html

Pontius, R. G., Jr., Boersma, W., Castella, J.-C., Clarke, K., de Nijs, T., Dietzel, C., Duan, Z., Fotsing, E., Goldstein, N., Kok, K., Koomen, E., Lippitt, C. D., McConnell, W., Mohd Sood, A., Pijanowski, B., Pithadia, S., Sweeney, S., Trung, T. N., Veldkamp, A. T., & Verburg, P. H. (2008). Comparing the input, output, and validation maps for several models of land change. The Annals of Regional Science, 42(1), 11–37. https://doi.org/10.1007/s00168-007-0138-2

Pontius, R. G., Jr., & Millones, M. (2011). Death to Kappa: Birth of quantity disagreement and allocation disagreement for accuracy assessment. International Journal of Remote Sensing, 32(15), 4407–4429. https://doi.org/10.1080/01431161.2011.552923

This open access article is distributed under a Creative Commons Attribution (CC-BY-NC) 4.0 license.

https://doi.org/10.35877/mathscience5506

ISSN : 2776-7922 (Print) / 2807-3037 (Online)

Pribadi, D. O., & Pauleit, S. (2015). The dynamics of peri-urban agriculture during rapid urbanization of Jabodetabek Metropolitan Area. Land Use Policy, 48, 13–24. https://doi.org/10.1016/j.landusepol.2015.05.009

Rondhi, M., Pratiwi, P. A., Handini, V. T., Sunartomo, A. F., & Budiman, S. A. (2018). Agricultural land conversion, land economic value, and sustainable agriculture: A case study in East Java, Indonesia. Land, 7(4), Article 148. https://doi.org/10.3390/land7040148

Schneider, A., Mertes, C. M., Tatem, A. J., Tan, B., Sulla-Menashe, D., Graves, S. J., Patel, N. N., Horton, J. A., Gaughan, A. E., Rollo, J. T., Schelly, I. H., Stevens, F. R., & Dastur, A. (2015). A new urban landscape in East–Southeast Asia, 2000–2010. Environmental Research Letters, 10(3), Article 034002. https://doi.org/10.1088/1748-9326/10/3/034002

Supriatna, S., Mukhtar, M. K., Wardani, K. K., Hashilah, F., & Manessa, M. D. M. (2022). CA-Markov chain model-based predictions of land cover: A case study of Banjarmasin City. Indonesian Journal of Geography, 54(3), 365–372. https://doi.org/10.22146/ijg.71721

Surya, B. (2016). Change phenomena of spatial physical in the dynamics of development in urban fringe area. Indonesian Journal of Geography, 48(2), 118–134. https://doi.org/10.22146/ijg.17631

Surya, B., Ahmad, D. N. A., Sakti, H. H., & Sahban, H. (2020). Land use change, spatial interaction, and sustainable development in the metropolitan urban areas, South Sulawesi Province, Indonesia. Land, 9(3), Article 95. https://doi.org/10.3390/land9030095

Surya, B., Salim, A., Hernita, H., Suriani, S., Menne, F., & Rasyidi, E. S. (2021). Land use change, urban agglomeration, and urban sprawl: A sustainable development perspective of Makassar City, Indonesia. Land, 10(6), Article 556. https://doi.org/10.3390/land10060556

Xu, H. (2006). Modification of normalised difference water index (NDWI) to enhance open water features in remotely sensed imagery. International Journal of Remote Sensing, 27(14), 3025–3033. https://doi.org/10.1080/01431160600589179

Zha, Y., Gao, J., & Ni, S. (2003). Use of normalized difference built-up index in automatically mapping urban areas from TM imagery. International Journal of Remote Sensing, 24(3), 583–594. https://doi.org/10.1080/01431160304987

This open access article is distributed under a Creative Commons Attribution (CC-BY-NC) 4.0 license.